The Role of Eddies in Determining the Structure and Response of the Wind-Driven Southern Hemisphere Overturning: Results from the Modeling Eddies in the Southern Ocean (MESO) Project

ROBERT HALLBERG AND ANAND GNANADESIKAN

NOAA/Geophysical Fluid Dynamics Laboratory, Princeton, New Jersey

(Manuscript received 8 October 2004, in final form 4 April 2006)

ABSTRACT

The Modeling Eddies in the Southern Ocean (MESO) project uses numerical sensitivity studies to examine the role played by Southern Ocean winds and eddies in determining the density structure of the global ocean and the magnitude and structure of the global overturning circulation. A hemispheric isopycnal-coordinate ocean model (which avoids numerical diapycnal diffusion) with realistic geometry is run with idealized forcing at a range of resolutions from coarse (2°) to eddy-permitting (1⁄6°). A comparison of coarse resolutions with fine resolutions indicates that explicit eddies affect both the structure of the overturning and the response of the overturning to wind stress changes. While the presence of resolved eddies does not greatly affect the prevailing qualitative picture of the ocean circulation, it alters the overturning cells involving the Southern Ocean transformation of dense deep waters and light waters of subtropical origin into intermediate waters. With resolved eddies, the surface-to-intermediate water cell extends farther southward by hundreds of kilometers and the deep-to-intermediate cell draws on comparatively lighter deep waters. The overturning response to changes in the winds is also sensitive to the presence of eddies. In noneddying simulations, changing the Ekman transport produces comparable changes in the overturning, much of it involving transformation of deep waters and resembling the mean circulation. In the eddy-permitting simulations, a significant fraction of the Ekman transport changes are compensated by eddy-induced transport drawing from lighter waters than does the mean overturning. This significant difference calls into question the ability of coarse-resolution ocean models to accurately capture the impact of changes in the Southern Ocean on the global ocean circulation.

1. Introduction

The water masses that compose the vast majority of the ocean volume are either formed, modified, or transit through the Southern Ocean (Sverdrup et al. 1942; Schmitz 1996; Doney et al. 1998). It has long been known that mesoscale eddies play an important role in the dynamics of this region (Johnson and Bryden 1989; Marshall et al. 1993; Killworth and Nanneh 1994; Marshall and Radko 2003). This paper explores how these eddies determine not only the magnitude and structure of water mass transformation but also its sensitivity to changes in surface wind stress. It demonstrates that mesoscale eddies play a critical role in determining the connection between the Southern Ocean momentum and buoyancy budgets.

In most of the ocean, zonal momentum input from surface winds to the light surface waters can be balanced by piling up these waters against a continent (Veronis 1996), limiting the wind-driven circulation to the surface layers. However, the Southern Ocean contains a band of latitudes where there is no continuous topography above a depth of about 1800 m. Strong eastward wind stresses impart momentum to the ocean driving a northward Ekman transport. In order for the mass budget to be closed, the northward flow must be supplied by southward-flowing waters. The equations of motion place some strong constraints on these flows. There can be no net geostrophic meridional flow averaged along any level surface above the depth of the ridges. The overturning in depth space thus requires a connection between northward-flowing surface waters and southward-flowing deep waters, leading to the "Deacon cell" with apparent upwelling throughout the

Corresponding author address: Dr. Robert Hallberg, NOAA/Geophysical Fluid Dynamics Laboratory, Princeton University Forrestal Campus, 201 Forrestal Rd., Princeton, NJ 08542.
E-mail: robert.hallberg@noaa.gov

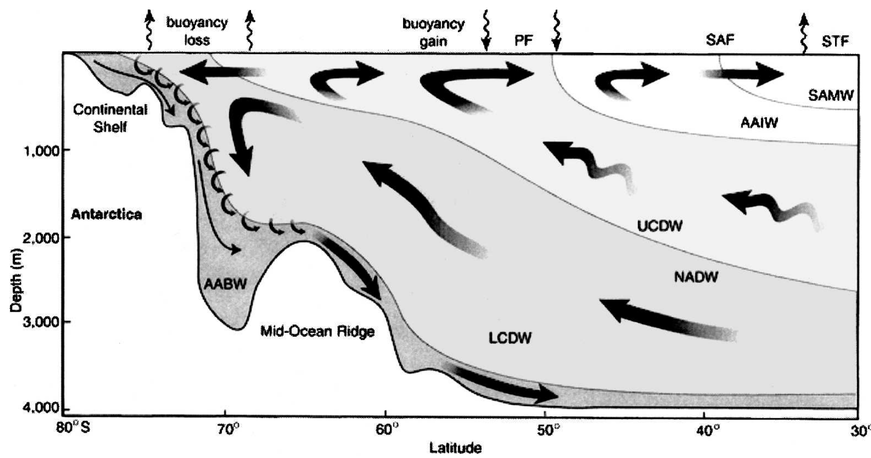

FIG. 1. Schematic of the hypothesized meridional circulation in the Southern Ocean from Speer et al. (2000).

Southern Ocean and deep apparent downwelling to the north of Drake Passage.

But as is widely recognized, depth–space overturning streamfunctions say nothing about the net transport of water masses. The net transport of water masses is much more accurately described in terms of overturning streamfunctions in potential density space,

$$\Psi(y, \rho) = \oint \int_0^{\rho} (vh)\, d\rho'\, dx\,,$$

where v is the meridional velocity and $h = -\partial z/\partial\rho$ is the thickness of isopycnal layers (e.g., Marshall 1997). Analyzing the circulation in density space essentially eliminates the northern downwelling branch of the Deacon cell (Döös and Webb 1994; Hirst and McDougall 1998). The upwelling branch, however, is more complicated.

Since the net transport in density space is the product of a velocity and a thickness, correlations between the two can result in a net geostrophic meridional eddy transport across the Antarctic Circumpolar Current (ACC), even in isopycnal layers that do not encounter either the ocean's surface or bottom. Poleward mass fluxes are associated with a divergence of eastward momentum fluxes, as found by Marshall et al. (1993) and Gille (1997). Theoretical formalisms such as the temporal residual mean (McDougall and McIntosh 2001) or the transformed Eulerian mean (TEM; Andrews and McIntyre 1976; Ferrari and Plumb 2003) cast the eddy transport into a form that isolates the eddy terms in the momentum, tracer transport, or continuity equations. All of these paradigms are equivalent at leading order to the density-space analysis used here, the principal difference being whether there appears to be a diapycnal eddy flux (as in TEM theory) or not (in density coordinates). In one limit, eddies spawned by the ACC pass the wind stress downward from layer to layer until it is taken up by bottom form drag, requiring no deep upwelling whatsoever (Johnson and Bryden 1989; Tansley and Marshall 2001). In this limit the Southern Ocean density-space overturning is independent of the Ekman transport.

An alternative is that the water that flows south below the level of the sills actually does upwell, is converted into Antarctic Surface Waters as a result of freshwater input, and flows northward in the Ekman layer (Warren et al. 1996; Toggweiler and Samuels 1998; Doney et al. 1998; Gnanadesikan and Hallberg 2000). Such a circulation requires substantial water mass transformation but does not require any process to flux momentum downward in the water column. In this limit, the overturning in density space is tightly linked to the wind stress and the density-space overturning streamfunction changes by the same amount as the Ekman transport (Gnanadesikan and Hallberg 2000).

The real Southern Ocean overturning, schematically illustrated in Fig. 1 (reproduced from Speer et al. 2000), is likely to sit between these two limits, of course. Some of the northward Ekman flux is supplied by upwelling of abyssal waters, which pass into the Antarctic below the depths of the ridges and some is supplied by southward flow of intermediate waters above the ridges (Döös and Webb 1994; MacCready and Rhines 2001; Hallberg and Gnanadesikan 2001; Karsten et al. 2002), while near-surface eddy fluxes help determine exactly which water masses are subducted (Marshall 1997). The sensitivity of the density-space overturning to wind changes will also likely lie between the two limits. However, it may differ from the mean balance, as transient eddies may compensate substantially more for changes in the Ekman transport than they do for the mean transport itself (Hallberg and Gnanadesikan 2001). The Southern Ocean response to forcing changes has not previously been examined in a realistic setting, except in scenarios where eddy effects are entirely or largely parameterized.

In large-scale ocean models, the effect of mesoscale eddies is often parameterized in terms of a diffusive tracer flux along isopycnals (Redi 1982; Griffies et al. 1998) and an advective flux resulting from a diffusive smoothing of isopycnal depths (Gent and McWilliams 1990; Gent et al. 1995; Visbeck et al. 1997). Both of these processes are governed by a lateral diffusion coefficient, which is often taken to be the same (Griffies 1998), and is typically calibrated to give a reasonable Southern Ocean density structure. But even models that are carefully calibrated to give a reasonable mean overturning circulation with a reasonable density structure are not guaranteed to respond correctly to forcing changes (Hallberg and Gnanadesikan 2001). This question of the Southern Ocean eddy response to forcing changes is of particular importance for the assessing the robustness of climate projections.

This manuscript presents the primary results from the Modeling Eddies in the Southern Ocean (MESO) project. MESO attempts to explicitly address the role of eddies in the Southern Ocean overturning circulation, and especially the sensitivity of that overturning circulation to wind forcing changes. As described in the next section, a hierarchy of model resolutions, all in a realistic domain covering the entire Southern Hemisphere and with a realistic mean state, is subjected to identical forcing perturbations. Comparison between the runs allows a clear indication of the effects of explicitly represented eddies and how these compare with a coarse-resolution parameterization. The ACC transport, eddy variability, and especially the density-space overturning streamfunction are all examined.

Explicit eddies affect the Southern Ocean overturning circulation in two ways that might not have been anticipated from previous realistic studies, although they have been suggested in more idealized contexts. First, eddies significantly extend the southward transport of relatively light water across the latitudes of ACC, with related increases in the poleward transport of heat. Second, with explicit eddies, the Southern Ocean overturning response to changing wind stresses is systematically smaller and its subsurface component expressed in shallower density classes than in models with parameterized eddies. These significant differences between models with explicit and parameterized eddies will be a challenge in developing better eddy parameterizations, and provide a clear impetus to develop a new class of coupled climate models that explicitly represent the ocean's mesoscale eddy field.

2. Methods

a. Physical model

The model used for these simulations is the primitive equation isopycnal coordinate model of Hallberg (1995). An isopycnal coordinate model is used for a number of reasons. First, fewer vertical degrees of freedom are required to represent internal wave modes and realistic topography relative to a level-coordinate model. Second, analysis of the model is much easier in water mass space—the framework used by observational physical oceanographers to discuss ocean circulation. Third, the cascade of variance to small scales does not lead to nonphysical diapycnal mixing, as is likely in a *Z*-coordinate model with vigorous eddies (Griffies et al. 2000).

The model solves the primitive equations in constant density layers. A three-way (barotropic, baroclinic, diabatic/tracer) split time-stepping scheme (Hallberg 1997) with subcycling of the shorter time steps assures that the model can be integrated efficiently while conserving momentum, mass, and tracers (by layer), potential vorticity, and energy (Arakawa and Hsu 1990). A monotonic, conservative tracer advection algorithm (based on Easter 1993) is used. The full nonlinear equation of state is used (Hallberg 2005; Sun et al. 1999). The model allows for turbulent entrainment in descending overflows and other regions of small resolved shear Richardson number, using the scheme of Hallberg (2000), but uses a weak diapycnal diffusivity of 10^{-5} m^2 s^{-1} elsewhere in the interior. The 20 interior layers are chosen to provide a reasonable resolution across the density range of the Southern Ocean and a limited resolution of the light water structure at low latitudes.

A three-layer bulk mixed layer (Hallberg 2003) is used. The mixed layer depth is determined by a turbulent kinetic energy budget, following a long tradition starting with Kraus and Turner (1967). This mixed layer is then divided into two sublayers, which are well mixed with respect to tracers but not with respect to velocity, allowing for shear-driven restratification. In addition, a parameterized restratifying circulation is also introduced to the mixed layer based on the horizontal density gradients (Hallberg 2003), to account for the fact that the viscous restratification would occur predominantly at smaller horizontal wavelengths than are resolved (Young 1994). As described by Hallberg (2003) in the absence of this shear-driven restratification mixed layer depths become excessively deep. A buffer layer below the mixed layer allows fluid to detrain smoothly into the interior (Thompson et al. 2002).

The low-resolution model runs (2° and 1°) use an interface height diffusion, which is the equivalent of the Gent and McWilliams (1990) (GM) eddy parameterization. Runs were made with a GM coefficient varying between 0 and 2000 $m^2 s^{-1}$. Only the runs with values of 0 and 1000 $m^2 s^{-1}$ are presented here, but the cited tendencies are consistent with those from the broader range. The higher-resolution models (½°, ¼°, and ⅙°) have no such parameterization. One run was made with the ½° model with GM to evaluate the impact of replacing the eddies with a parameterized representation of their effects. The biharmonic Smagorinsky viscosity of Griffies and Hallberg (2000) is used to provide a momentum closure, removing enstrophy at small scales without substantially affecting the large-scale dynamics.

b. Experimental design

MESO consists of a series of simulations at different horizontal resolutions (2°, 1°, ½°, ¼°, and ⅙°). MESO covers the entire Southern Hemisphere with a Mercator grid; the north–south resolution increases poleward to keep the grid boxes square. Thus, at 60°S the ½° model has a grid spacing of 27.8 km, while the ⅙° resolution is 9.3 km. Topography was generated using the dataset of Smith and Sandwell (1997) averaged to the grid resolution. All resolutions thus can be said to have "realistic" topography, though clearly the highest-resolution cases are the most accurate.

Boundary conditions at the northern boundary are handled by applying strong sponges with a restoring time scale that is short in comparison with the Atlantic crossing time of the first internal-mode equatorial Kelvin wave. The equator was chosen for the northern boundary as it is the only latitude where it is possible to specify density fields without specifying normal velocities (away from the equator, geostrophy dictates that density fields and velocity fields are strongly linked). Using strong sponges means that the mean state of the model is constrained to remain close to the real world and ensures that much of the spinup occurs in less than 20 yr. It also ensures that changes in the Southern Ocean circulation are driven by local changes and not by inaccurate water mass formation in the North Atlantic. But it precludes the significant changes in the pycnocline depth throughout the global ocean that the Southern Ocean wind stress changes might otherwise produce (McDermott 1996; Toggweiler and Samuels 1998; Gnanadesikan and Hallberg 2000). Weak sponges are applied around the Antarctic ice shelves to ensure the formation of Antarctic Bottom Water. While the details of these Antarctic shelf sponges can influence the formation rates of Antarctic Bottom Water and even the net transport of the ACC (through the thermal wind relationship starting from a weak flow at the bottom), low-resolution tests with differing specifications for these sponges show very similar changes in response to the wind stress changes, which is the focus of this paper.

A significant effort was made to come up with plausible buoyancy fluxes for the Southern Ocean. Existing reanalysis products are only loosely constrained by the few observations. By contrast, the sea surface temperature and salinity are relatively well observed and so may be used to diagnose heat and salt fluxes. An overly strong restoring has the effect of damping out eddy variability. An adaptive procedure for diagnosing the ocean heat and freshwater fluxes is described in the appendix. This scheme allows for the fluxes to adjust to the circulation during the spinup period, while keeping the model near the climatological surface temperature and salinity. In the zonal mean, the surface heat fluxes are plausible (Fig. 2), and the implied meridional heat transport is within the range that can be deduced from atmospheric reanalysis and satellite observations (Trenberth and Caron 2001). However, some aspects of the exact spatial distribution (such as a very large heat loss from the East Australia Current Extension) are not plausible.

The models are run for 20 yr in a spinup period and for 20 yr (25 at ⅙°) during the main experiment. During each period the wind stress is kept fixed (there is no seasonal cycle). The baseline wind stress produces the Ekman flux shown in Fig. 3. The flux peaks at around 46°S with a northward transport of 55 Sv (1 Sv $\equiv 10^6$ $m^3 s^{-1}$).

After the spinup period, the buoyancy forcing was fixed (apart from a weak feedback of temperature anomalies on the heat fluxes of 20 W m^{-2} K^{-1} and an equivalent weak feedback on surface salinity), and three separate runs were started. Based on bulk formulas, 20 W m^{-2} K^{-1} is a plausible feedback of heat fluxes on SST anomalies. In one case, (referred to as "middle winds") the wind stress is left unperturbed. Two other cases were started in which the wind stress was increased by 20% ("high winds") or decreased by 20% ("low winds"). This is equivalent to a peak change in the Ekman transport of about 11 Sv. Renwick (2004) suggests that winds over the Southern Ocean may have increased by about this amount since 1980. The fact that

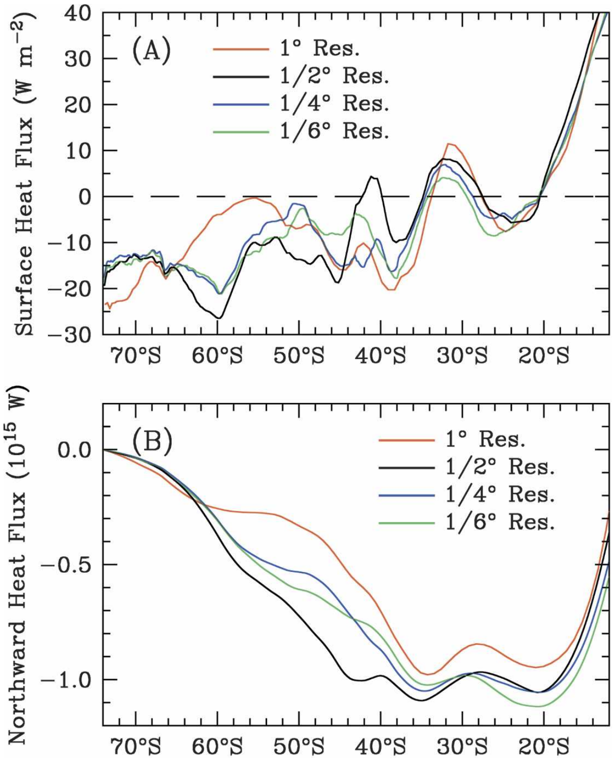

FIG. 2. (a) Zonal mean surface heat fluxes into the ocean and (b) zonally integrated northward ocean heat transport at different resolutions. The ocean model transports heat southward at all latitudes for all resolutions, but with much larger southward heat fluxes across the ACC in the eddy-permitting models than in the 1° model with parameterized eddies.

the forcing remains constant (there is no annual cycle) ensures that all variability is intrinsic to the model. It also allows us to assess changes in the eddy field and the mean circulation in a statistically meaningful way using feasibly short runs.

It is helpful to put these simulations in the context of other fine-resolution studies of the Antarctic such as the Fine Resolution Antarctic Model (FRAM; Stevens and Ivchenko 1997; Killworth and Nanneh 1994) and the "quarter degree" model of Semtner and Chervin (1992) used by Gille (1997) to examine the momentum balance of the Southern Ocean. Using the same terminology as here, the Semtner–Chervin model would be a 0.4° model and FRAM would be a ½° model. The spinup at high resolution here is much longer than the spinups in either of these models. More recent simulations have been carried out at higher horizontal resolutions than FRAM [e.g., Best et al. (1999) at 9⁄32° resolution], but a detailed study of the response of the flow to changes in surface forcing in such models has not been done.

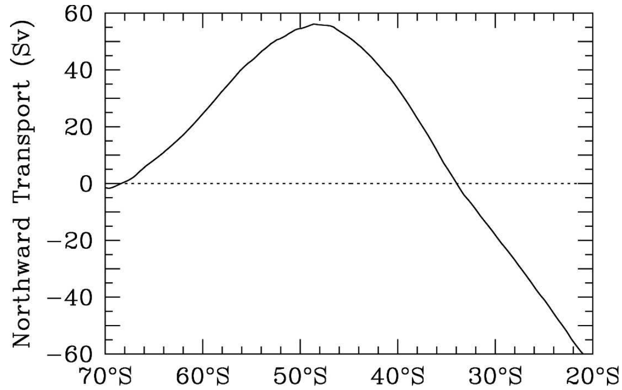

FIG. 3. Zonally integrated northward Ekman transport $\int(\tau/\rho_o f)\,dx$ with middle winds. With high winds this transport is increased by 20%. With low winds it is decreased by 20%.

3. Results

a. Circulation of the central cases

1) ZONAL TRANSPORT

A standard diagnostic of the Southern Ocean circulation is the transport of the ACC though Drake Passage, the time series of which are shown in Fig. 4 for four different resolutions. The observed transport varies between 110 and 150 Sv (Whitworth et al. 1982; Cunningham et al. 2003). The simulations tend to lie on the high side of this number, but are substantially lower than the 200 Sv found in the simulation of Semtner and Chervin (1992) and the 0.5° FRAM simulation of Killworth and Nanneh (1994). Refining horizontal resolution results in a decrease in the transport as eddies become increasingly energetic. The transport stabilizes after a few years in both the spinup and the perturbation runs. The 1° runs, which include parameterized eddy effects, are able to match the mean transport, and to a lesser extent the sensitivity of the mean transport seen in the ¼° runs. However, when the runs are examined in detail, it can be seen that the separation between high, medium, and low wind stress cases that is so clear in the low-resolution (1° and ½°) simulations is much smaller and less clear in the ⅙° simulations. The response of the current to changes in winds when eddies are represented explicitly is significantly smaller than when they are parameterized. Low-resolution simulations with different values of the GM thickness diffusivity (not shown) exhibit roughly the same range in the response of the Drake Passage transport to wind changes, despite very different mean transports. The Drake Passage transport response is likely to be difficult to capture exactly without simulating the eddies directly.

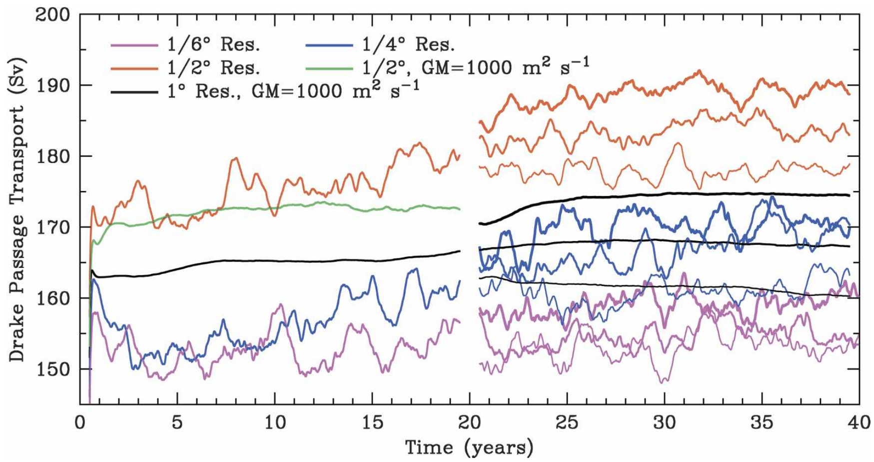

FIG. 4. One-year running mean Drake Passage transport at ⅙° (magenta), ¼° (blue), and ½° (red) resolutions with explicit eddies, and at ½° (green) and 1° (black) resolutions with eddy effects parameterized with an interface height diffusivity (akin to GM) of 1000 $m^2 s^{-1}$. After 20 yr, the heavier lines denote the cases with stronger winds and the thinner lines are with weaker winds. Adding the GM parameterization to the ½° model suppresses both the marginally resolved eddy variability and most of the Drake Passage transport variability at a range of time scales.

The inclusion of eddies results in large variability in the Drake Passage transport even though the forcing is steady. The variability has large amplitude on a range of time scales, with a weekly peak-to-trough range of 30 Sv, down to a 5–10-Sv range in the 1-yr low-pass-filtered transport (Fig. 4). The ½° run with GM suppresses most of this variability, indicating that it is truly a function of the presence of eddies rather than being due to the resolution.

2) EDDY FIELD

The realism of the simulated eddy field can be assessed by comparing the RMS sea surface height (SSH) variability with altimeter data (Fig. 5). The model captures the large-scale features in the data, including the high variability off of South Africa associated with the shedding of Agulhas eddies, the southward trend of variability associated with the Southern Drift of the ACC, the extension of the variability to the north around Campbell Plateau and the high-variability region off of Argentina. Additionally the model captures some midlatitude features such as the extension of high SSH variability off Queensland, Australia, into the ocean interior. Detailed quantitative comparisons can be somewhat misleading, as the model has no variability in the forcing, while the Ocean Topography Experiment (TOPEX) data reflect such atmospheric forcing variability, leading to much greater SSH variability in regions of low eddy activity. The ⅙° model (Fig. 5a) shows little change between the last 5 yr of the spinup and the last 5 yr of the experiment period with the same winds, indicating the eddy field is in rough equilibrium. The ⅙° model is somewhat more energetic than the ¼° model (Fig. 5b), particularly in energetic boundary current regions. The difference is not large, and a zonal average of the squared SSH anomalies indicates that in the Southern Ocean the ⅙° model is about 30% more energetic than the ¼° model, but a factor of 3 more energetic than the ½° model.

Another signature of these differences can be seen in snapshots of the surface speed (Fig. 6). The overall structure of the two fields is very similar, but the ⅙° model shows clear evidence of eddies at all locations. Particularly noticeable in these simulations are the closed rings associated with Agulhas eddy shedding and the loops in the East Australian and Brazil Currents. Animations of these simulations show these loops moving southward along the coast until they reach a separation point at which they drift into the interior. In the interior, the high-resolution simulations show that the current breaks down into individual jets, as found by Rhines (1977) in idealized simulations of geostrophic turbulence. As in the idealized simulations of Hallberg and Gnanadesikan (2001) these jets appear to form downstream of topography and then disappear as the current moves around such features as the Kerguélen and Campbell Plateaus and Drake Passage. Away from the boundary currents, there is also a clear sense of

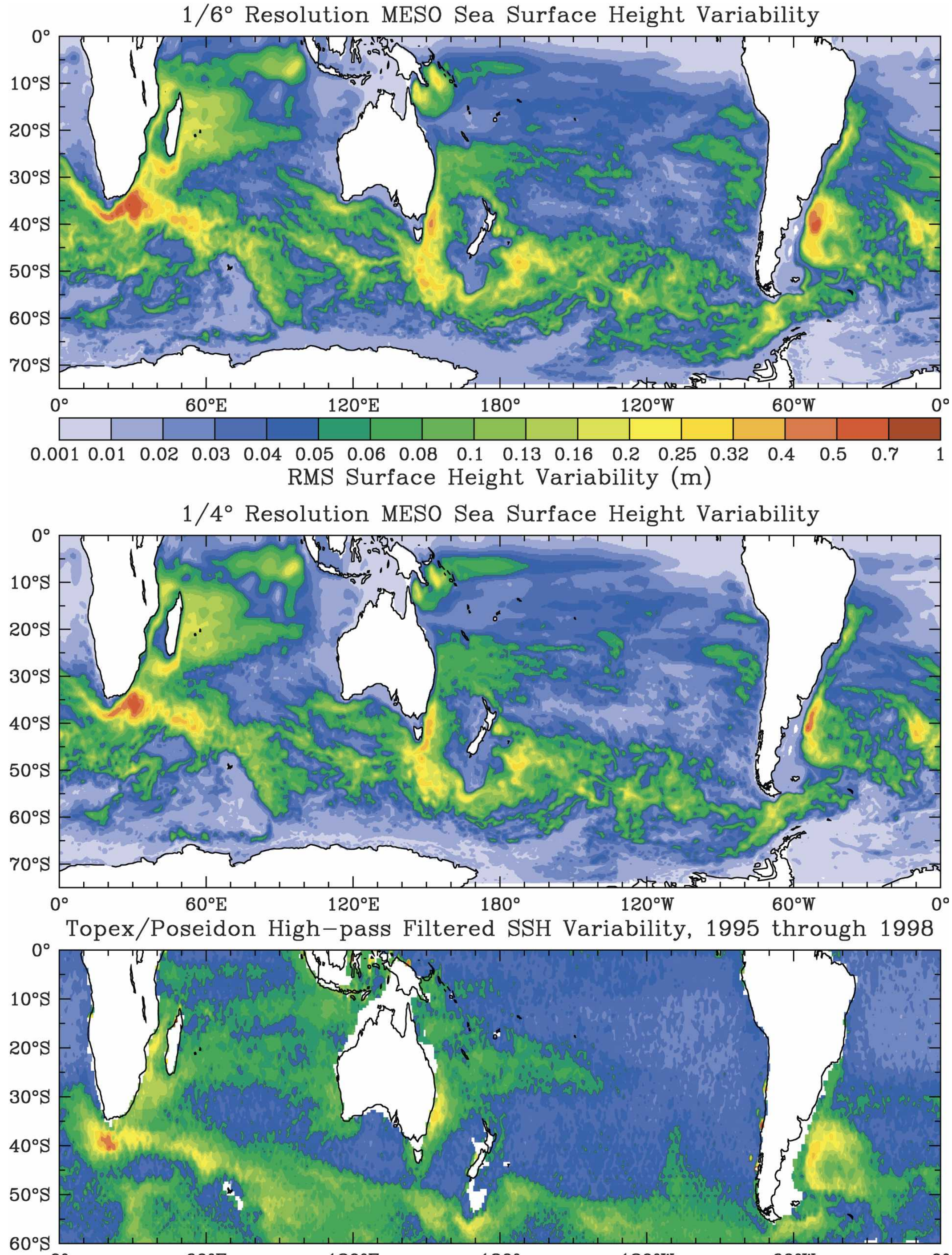

FIG. 5. RMS SSH variability from the (top) ⅙° model and (middle) ¼° model, both with middle winds averaged over years 35–40, and (bottom) the RMS of TOPEX/Poseidon SSH anomalies on a ½° grid, 90-day high-pass filtered to remove the seasonal cycle, from 1995 to 1998.

smaller scales (too small to be seen clearly in this hemispheric view) appearing as one moves to higher latitudes, consistent with changes in the internal deformation radius.

3) Meridional overturning streamfunction

The meridional overturning streamfunction in density space contains three principal cells (Fig. 7). The red

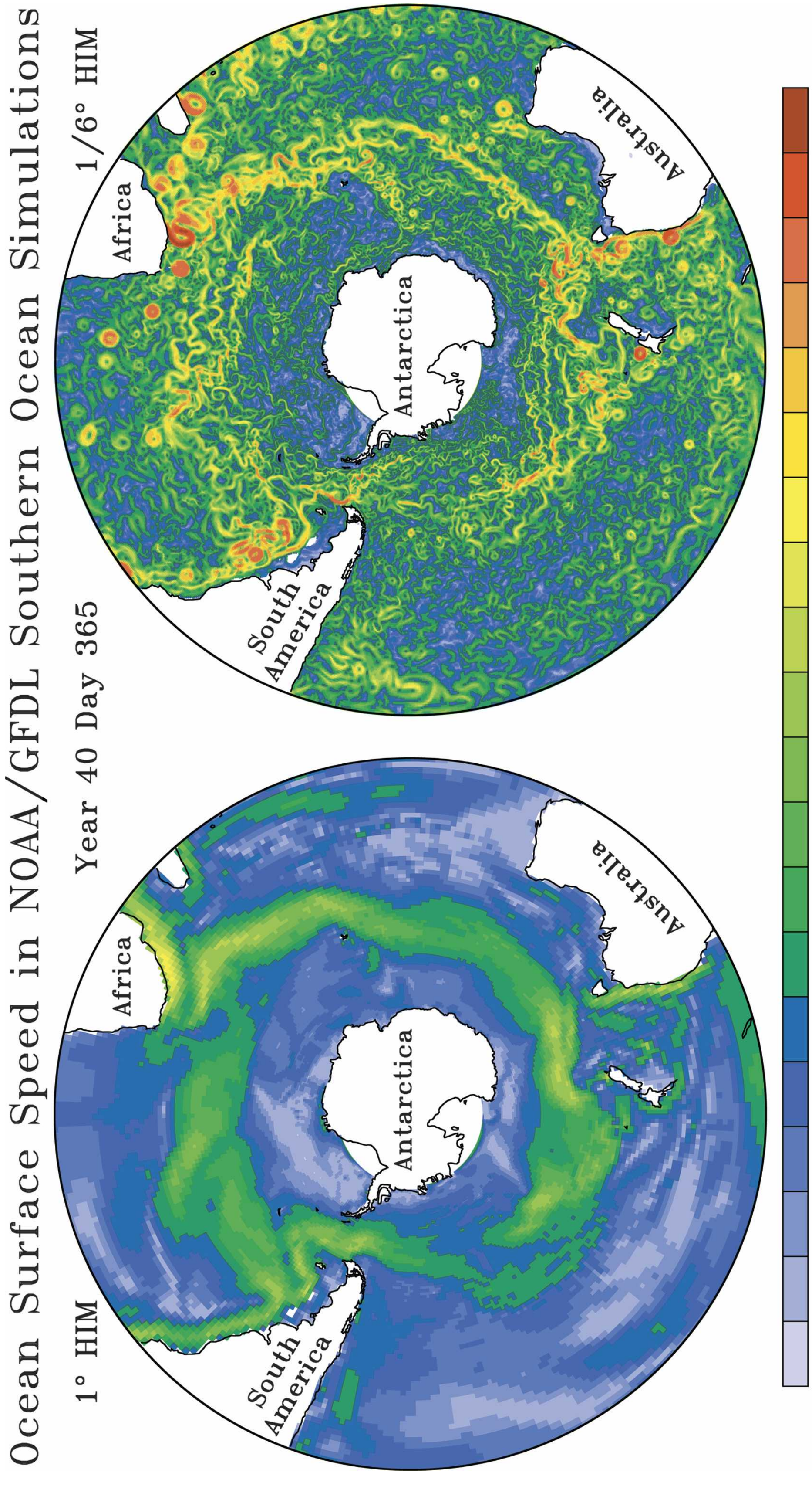

FIG. 6. Instantaneous surface speed in 1° and 1/6° models after 40 yr. Note that the large-scale structure of the 1° model is quite similar to the 1/6° model (the currents have similar locations and have similar horizontal extents). The main difference is in the presence of intense jets and eddies in the 1/6° model.

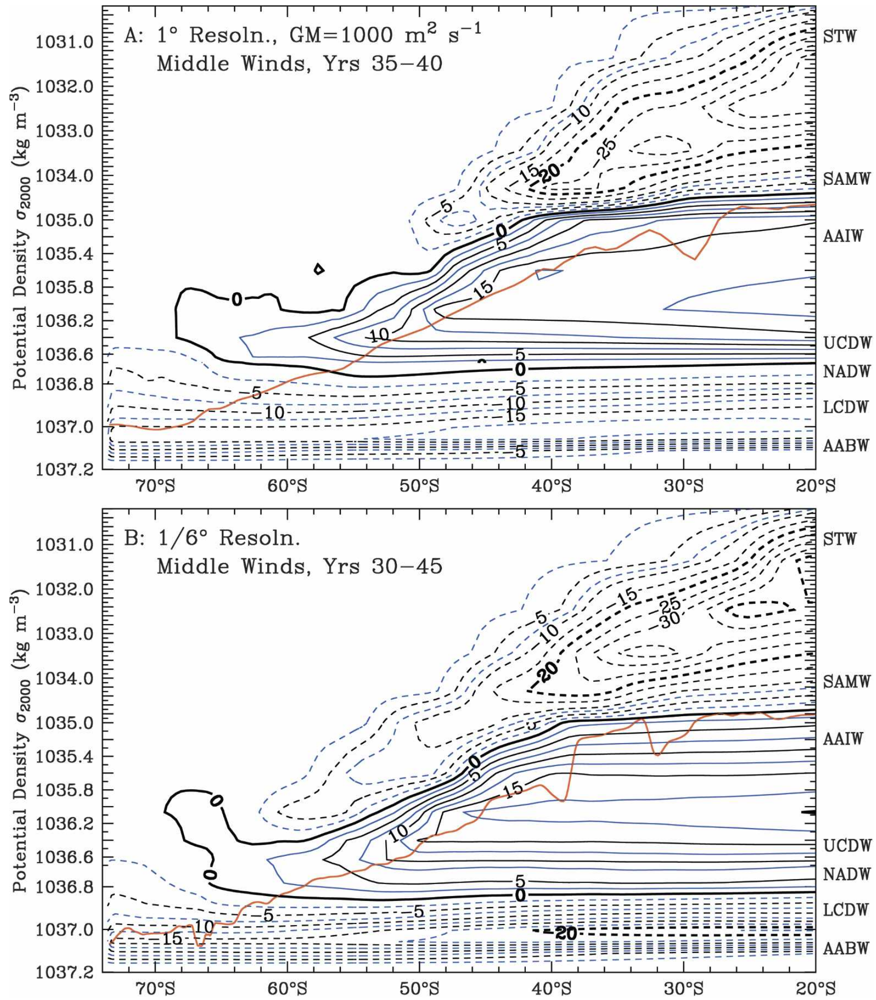

FIG. 7. Density-space overturning streamfunction at (a) 1° and (b) ⅙°. Positive values (solid lines) indicate cells that flow clockwise, while negative values (dashed lines) flow counterclockwise. The black lines use a 5-Sv contour interval, augmented by blue contours at a 2.5-Sv interval (except below −10 Sv in the subtropical cell). The red lines show the zonal maximum time-averaged density of the top 50 m. Circulation above this level can have contributions from the mixed layer. Water masses [as in Fig. 1 with the addition of subtropical water (STW)] are shown at right. The ⅙° resolution model is averaged over 15 yr, not 5, because of its much greater low-frequency variability.

line approximately shows the densest water found in the mixed layer, so that any flow above this line is occurring partially in the mixed layer. Below this line, vertical flow can either be due to diapycnal mixing or to changes in the volume of particular layers. The flow shows many of the same features as the conceptual outline in Fig. 1, but with one major difference—there is a strong flow of relatively light surface waters into the Southern Ocean. In the 1° model (Fig. 7a) approximately 15 Sv of light water crosses 40°S. These locally "light" waters are increasingly cold and dense farther to the south, with the southward extent of this light branch in density space reflecting the extent of the intensely cooling southward western boundary currents off South America and Australia. Most of this water is rapidly transformed into Sub-Antarctic Mode Water (SAMW). Below this is a cell in which about 18 Sv of North Atlantic Deep Water (NADW) and Common Deep Water upwell into the mixed layer, and are transformed into Antarctic Intermediate Water (AAIW). Below this there is a strong cell by which Circumpolar Deep Waters are transformed into Antarctic Bottom Waters. The great bulk of the water mass transformation occurs on density surfaces that are in or near the mixed layer (above the red line). Neither the 1° model nor the ⅙° model exhibits the overturning streamfunction feature known as the Deacon cell, a common Southern Ocean averaging artifact in depth–space overturning streamfunctions arising from cancellations above the shallowest topography of northward and southward geostrophic flows at the same depth but different densities (Döös and Webb 1994; Hirst and McDougall 1998).

The circulation at ⅙° resolution has a similar qualitative structure (Fig. 7b) as the 1° solution. This is reassuring, as it indicates that the coarse models do have some skill in simulating the large-scale overturning circulation within the Southern Ocean. The cell involving the NADW and AAIW is very similar in the two models, and is in fact slightly stronger in the ⅙° model. The major difference is that the surface cell extends much farther to the south. Whereas in the 1° model only 5 Sv of light surface water cross 44°S and mostly are converted to SAMW by 50°S, in the ⅙° model more than 10 Sv cross 44°S, half of which reaches a latitude of 58°S. This contrast in the overturning circulation is also reflected in the diagnosed mean heat transport (Fig. 2b), with a significantly greater poleward heat transport in these latitudes in the ⅙° model.

It is perhaps counterintuitive that the surface cell has a net southward transport of the lightest waters even in latitudes (50°–30°S) where the Ekman transport is northward. Karsten and Marshall (2002) diagnose a similar southward flow of 8 Sv of the lightest waters across 50°S, and extending to about 54°S, in their TEM analysis of the overturning circulation combining satellite observations of eddy activity and the time-mean observed interior state. This cell is present even in the 1° model, in which it corresponds to a southward transport of warm water in boundary currents and entrainment of this water into the ACC, where it cools and flows northward in the interior Ekman layer. This surface cell highlights the danger of thinking about the Circumpolar Current region in purely two-dimensional terms.

In the ⅙° model, coherent eddies and localized persistent meanders carry warm waters much farther poleward (up to 60°S), so that the lightest water is moving southward throughout the entire circumpolar band. Figure 8 shows a breakdown of the flow of this light water into time-mean and transient eddy components at 55° and 60°S integrated over longitude. Comparison of the time-mean surface density between the two resolutions (the red and black lines in Fig. 9), shows that at least some of the greater southward transport of light waters at higher resolution is due to persistent poleward meanders of the intense topographically constrained boundary currents in the high-resolution model, for example at 60°S, 170°E. But while the mean flow does bring light water into the Southern Ocean, most of this light water is returned in northward-flowing mean currents (Fig. 8), especially at 60°S. The net transport is dominated by transient eddies. At 60°S roughly 4 Sv of the lightest flow are due to transient eddies, while 1.2 Sv is due to the mean flow.

The nature of the southward transient eddy fluxes is more explicitly evident in Fig. 9, which superimposes them on the mean surface densities at 55° and 60°S. The largest contributions come to the east of the major topographically induced excursions near Campbell Plateau (165°E) and Drake Passage (70°W)—these are essentially surges in the boundary currents, often associated with the large coherent loops visible in Fig. 6. There are several regions with southward eddy transport of water that is substantially lighter than the mean values, for example around 130°W at 60°S and the small southward transports in the lee of Kerguélen (80°E). These are the oceanic equivalent of the wintertime cold air outbreaks described by Held and Schneider (1999) in their characterization of the isentropic overturning of the atmosphere. But the ACC has significant eddy variability throughout its course, and there is a nonnegligible southward transient eddy transport of light water distributed across the southeast Pacific.

The Falklands Current contributes a significant fraction of the globally integrated net southward transient eddy transport of light waters at between 55° and 60°S; this is examined in detail in Fig. 10. At 55°S the transport of light water associated with the mean flow ($\int\int \overline{v}\overline{h}\ dx\ d\rho$) is 33.5 Sv northward, while the actual mean ($\int\int \overline{vh}\ dx\ d\rho$) is 31 Sv, giving a 2.5-Sv southward flow associated with the large variability seen in Fig. 10a. Note that the mean flow of light water is northward throughout this entire region (Fig. 10b) and that the layer thickness gradients are large in many locations. A composite analysis of the thickness and flow anomalies during periods of anomalously southward and northward transport indicates that the mechanism that accomplishes the eddy transport is related to the shedding of eddies near the North Scotia Ridge. Under anomalously southward flow conditions (Fig. 10c), the eddy tends to form to the south of the ridge. It subsequently propagates eastward and is eroded by surface fluxes. During periods of strongly northward light flow (Fig. 10d), the height anomaly has the opposite sign and there is a hint of an eddy forming along the ridge. The flows involved in these eddies are large in comparison with the 2.5-Sv net flow involved and are very heterogeneous. These analyses give a clear indication of the importance of coherent eddies in extending the southward transport of light waters in the high-resolution

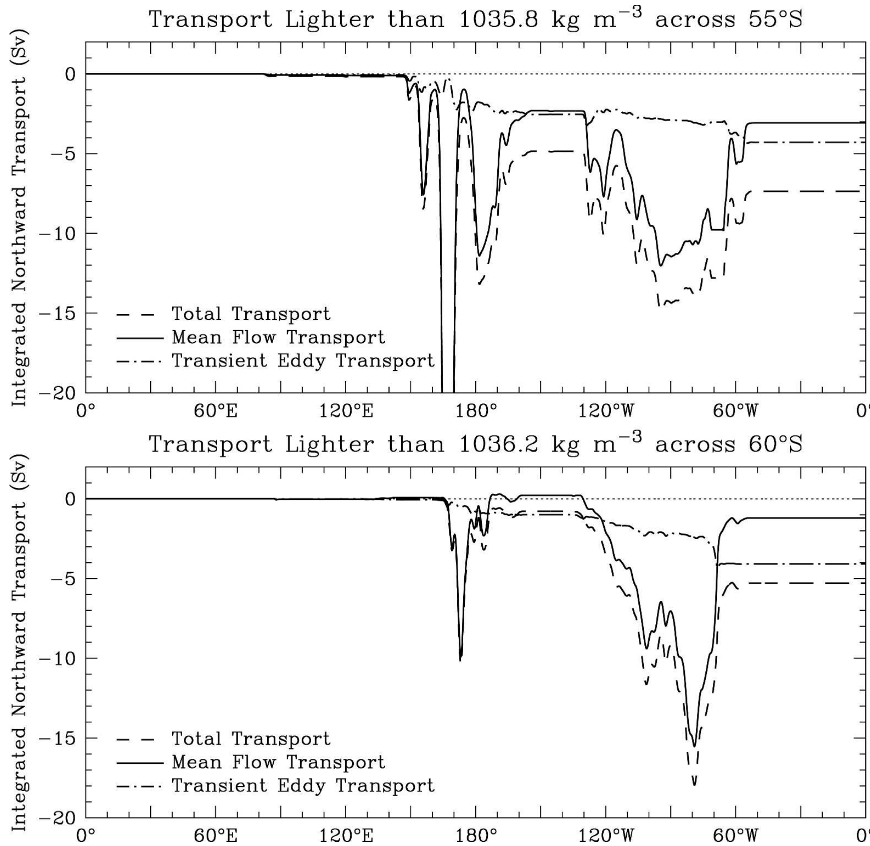

FIG. 8. (top) A breakdown of the flow of water lighter than σ_{2000} = 1035.8 kg m^{-3} across 55°S and (bottom) lighter than σ_{2000} = 1036.2 kg m^{-3} across 60°S into time-mean ($\int\int_0^x \overline{v}\overline{h}\, dx'\, d\rho$) and transient eddy ($\int\int_0^x \overline{v'h'}\, dx'\, d\rho$) components, along with the total meridional transport of these light waters, for years 35–40 of the ⅙° model with middle winds. Here the overbars are time means and the primes are deviations from those means.

models as compared with their low-resolution counterpart.

b. Response to wind stress changes

1) ZONAL TRANSPORT RESPONSE TO WIND STRESS

Changing the surface winds has a modest effect on the Drake Passage transport (Fig. 4). The largest impact is seen in the 1° model, with changes up to 8 Sv relative to a mean of 165 Sv (less than 5%). The ⅙° run shows much smaller and less consistent changes. Taken together, the runs show that a wind stress change of 20% produces a transport change of around 3%–5%. Consistent with the small change in transport, the zonal mean sea surface height also shows very little change as a result of the change in wind stress (Fig. 11a). The changes are only a few centimeters out of the 2-m drop across the ACC. This small response is consistent with arguments put forward by Marshall et al. (1993) that the ACC should accelerate until it is baroclinically unstable. It is important to remember, however, that the damping of the density at the equator means that the mechanism for changing Drake Passage transport outlined in Gnanadesikan and Hallberg (2000) (viz., an increase in the depth of the warm water sphere) has limited applicability in these simulations. Even were the damping not used, it is unlikely there would be a significant response in the global mean subtropical thermocline depth within the 20 yr covered by these runs.

2) EDDY FIELD RESPONSE TO WIND STRESS

The eddy field, by contrast, has a much more linear response to changes in wind stress. Figure 11b illustrates that increasing the wind stress increases the mean square SSH variability and decreasing the wind stress decreases the SSH variability within the core of the ACC. The shape of the change is consistent with the baseline SSH variability. The changes from increasing or decreasing the winds by 20% almost lie on top of

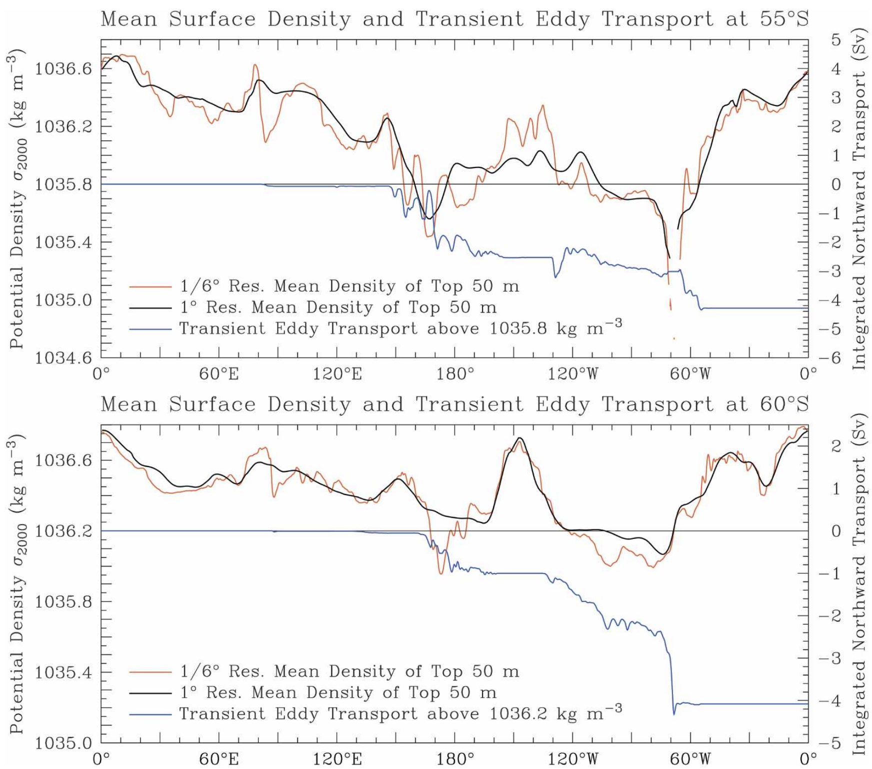

FIG. 9. The time-mean surface density in years 35–40 of the 1° (black) and ⅙° (red) models along (top) 55°S and (bottom) 60°S, along with the zonally integrated transient eddy flux ($\int\int_0^x \overline{v'h'}\, dx'\, d\rho$) of light waters across these latitudes (blue). The transport is calculated for water lighter than the horizontal black lines.

each other and nearly coincide with 20% of the value from the middle winds case, suggesting a linear response of the eddy energy to wind stress. Such a response was also found in Hallberg and Gnanadesikan (2001). It is consistent with a simple balance in which eddy kinetic energy dissipation goes as E/T (where E is the energy and T is a scale time for dissipation) and eddy kinetic energy generation is proportional to the wind work, $\boldsymbol{\tau} \cdot \mathbf{u}$, where $\boldsymbol{\tau}$ is the wind stress and $\mathbf{u}$ the surface velocity. Since, as was already noted, $\mathbf{u}$ is roughly constant, if T is also constant, $E \sim \|\boldsymbol{\tau}\|$.

Many regions where the eddy kinetic energy (EKE) changes (Fig. 12) are associated with boundary currents or topographic features. There is an increase in the EKE off Madagascar, Tasmania, the North Island of New Zealand, Campbell Plateau, where the ACC goes over the mid-Pacific ridge, and in the Brazil Current. Not all places, however, where the EKE is high exhibit an increase in EKE. For example the Agulhas retroflection does not show a strong increase in EKE. In general, the largest changes in EKE are found at the Subantarctic Front, rather than at the polar front lying farther south. Similarly, off Kerguélen Plateau the EKE is high, but does not change significantly with increasing winds.

3) MERIDIONAL OVERTURNING STREAMFUNCTION RESPONSE TO WIND STRESS

The overturning streamfunction generally responds to the increasing wind stress with an amplification of the surface-to-mode water and deep-to-intermediate cells, and minimal change in the abyssal northward flow of Antarctic Bottom Water (Fig. 13). The surface-to-mode water cell increases by about 20% at all resolutions. The intermediate cell in the 1° model increases by about 30% (up to 7 Sv out of ~24). South of about 40°S, the middle overturning cell accounts for the bulk of the change. Of the 7-Sv change, 5 Sv comes from water denser than 1036.8, nominally dense Lower Circumpolar Deep Water. In the 1° model, a large fraction of the change in zonally integrated Ekman transport (9 Sv at 55°S; see Fig. 3) is supplied from deep upwelling. The degree of intensification in the ⅙° model is quite different from the 1° model. While the shallow cell intensifies by about 20% as in the 1° model, the changes

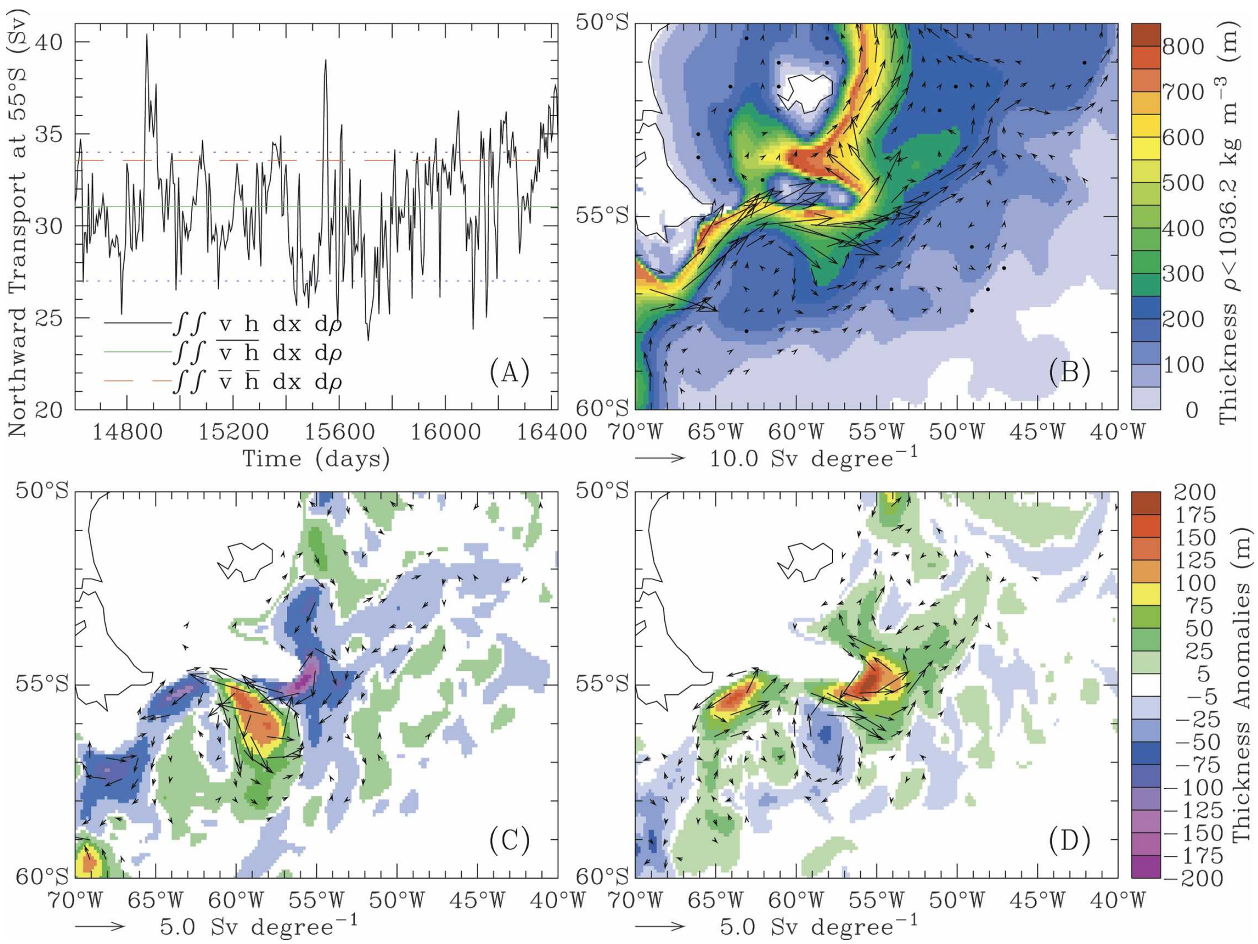

FIG. 10. The transport of water lighter than 1036.2 kg m^{-3} in the Falkland Current. (a) The time series of meridional transport across 55°S, along with lines showing the time mean transport (green) and the transport due to the mean velocities and thicknesses (red dashed). (b) The mean thickness of water lighter than 1036.2 kg m^{-3}, along with the mean transport of this light water. Composites of the thickness and transport of light water when the northward transport of this water across 55°S is (c) less than 27 or (d) more than 34 Sv. These flow levels are shown with dotted blue lines in (a).

in the deep/intermediate cell are noticeably weaker and shallower at ⅙° than at 1° resolution.

This difference in the overturning response can be seen more clearly in Fig. 14, which illustrates the overturning streamfunction change for three different resolutions at 30°, 40°, and 50°S. The change in the deeper overturning cell (the conversion of deep waters into intermediate) is substantially smaller at the higher resolutions. At the peak, the deep response to increased winds is roughly 4.5 Sv at ⅙° resolution, as compared with 7 Sv at 1°. This result is systematic and robust. It appears for both strengthening and weakening winds. The ¼° resolution is clearly intermediate between the 1° and ⅙° resolutions, reflecting the presence of eddies, but at a lower intensity than in the higher-resolution model. Moreover, although 15-yr averages are shown in Fig. 14, the same trends appear in every pentad.

There is an asymmetry between the cases with the strengthening and weakening winds, with the weakening winds showing less difference between resolutions. The asymmetry is evident in both the magnitude of the overturning changes, and in the depth at which the changes occur. For Fig. 14c, the increase in the deep cell overturning is 3.6 Sv for increased winds as compared with 5 Sv for weakening winds. This asymmetry is consistent with the idea that eddies act to limit the shears, and as they become stronger they are increasingly able to compensate for forcing changes, as illustrated in the idealized study of Hallberg and Gnanadesikan (2001). Even the highest-resolution simulations are clearly not converged. Extrapolating from the simulations presented here, the true ocean might be expected to exhibit even greater asymmetry between strengthening and weakening winds and an even greater eddy compensation for changes in the Ekman transport.

The deep (southward flowing) overturning response

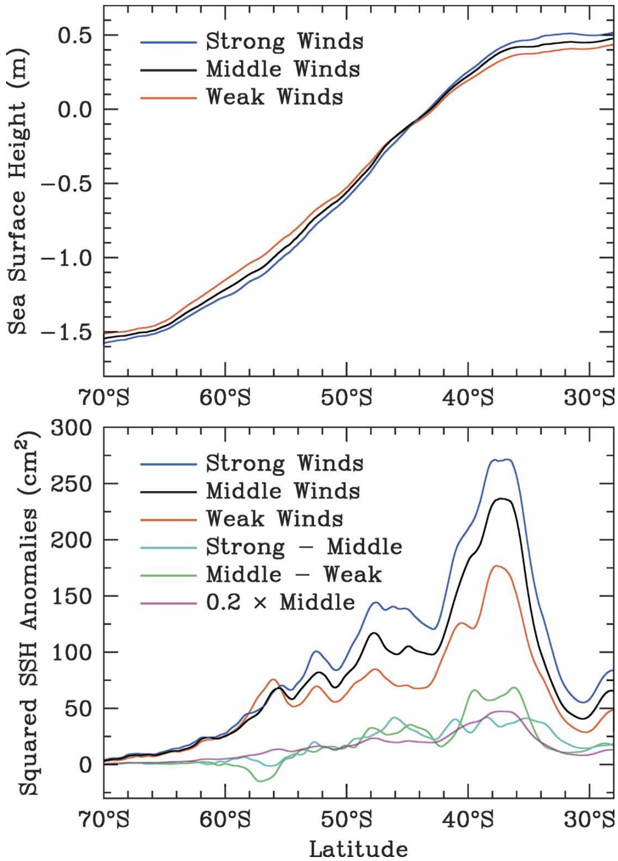

FIG. 11. SSH responses to changing winds in the ⅙° model, averaged over years 30–45. (top) Zonal-mean SSH, showing that the changes are small in comparison with the 2-m drop across the ACC. (bottom) The change in the mean squared SSH temporal anomalies resulting from the wind stress changes. The changes here are essentially linear with the wind stress magnitude, as shown by the near agreement between the green, cyan, and magenta lines.

occurs in systematically lighter, shallower waters at higher resolutions. This can be seen most clearly in the density-space overturning presented in Fig. 14c, which has a smaller range of density in its vertical axis, but it is also present in Figs. 14a,b. In this figure, there is almost a 4-Sv change in the southward flow of waters denser than 1037 in the 1° model, but none at higher resolutions. Recasting the overturning in "nominal depth" space (using the average depth of the isopycnal surface as the vertical coordinate instead of potential density, giving the temporal residual mean streamfunction; McDougall and McIntosh 2001) the results are even more dramatic (Fig. 14d). When eddies are resolved the response of the overturning circulation is concentrated on shallower isopycnals. This is consistent with the idea, shown graphically in Fig. 1 (adopted from Speer et al. 2000), that eddies allow for mass fluxes above the level of topography, which can feed a significant portion of the surface Ekman flux.

It is useful to contrast this behavior with that of the overturning associated with the wind-driven subtropical gyres. At 30°S the response of the upper cell (corresponding to the wind-driven gyres) is hardly affected by the model resolution, suggesting that eddies will have a relatively small direct impact on the tropical heat transport associated with the wind-driven gyres. This is consistent with coarse-resolution studies (such as Gnanadesikan et al. 2003), which show that changing the lateral eddy mixing coefficient has a large effect on the transport of heat across the Southern Ocean, and a moderate effect on the transport of heat between the Southern and Northern Hemispheres, but a minor impact on the export of heat from the Tropics.

c. *Summary of results*

In summary, these simulations show that resolving eddies can significantly alter the circulation of the Southern Ocean and its response to changes in forcing. Resolving eddies produces changes in the transport and variability of the ACC, results in extending the flow and transformation of relatively light waters much farther south, attenuates the response of the overturning circulation to changes in wind stress, and results in the surface Ekman flow being fed from much shallower depths. Since this Ekman flow feeds interior flows of water that penetrate into the low-latitude thermocline, even influencing equatorial upwelling, Southern Ocean eddies can have global effects.

4. Discussion

a. *Southern Ocean winds and the overturning circulation*

One important question upon which these results have some bearing is the role of surface winds in driving the global overturning circulation. There are currently two strains of discussion regarding how the overturning is driven—both largely based on circulation models at various levels of idealization. In the picture of Bryan (1987), Klinger and Marotzke (1999), and Klinger et al. (2003) it is low-latitude diffusion that closes and drives the circulation. By contrast, a number of papers have found that Southern Ocean winds (Toggweiler and Samuels 1993, 1998; Gnanadesikan 1999; Gnanadesikan and Hallberg 2000; Nof 2000; Toggweiler and Bjornsson 2000; Gent et al. 2001; Karsten et al. 2002), surface temperatures (Vallis 2000), eddies (Gnanadesikan 1999; Karsten et al. 2002; Gnanadesikan et al.

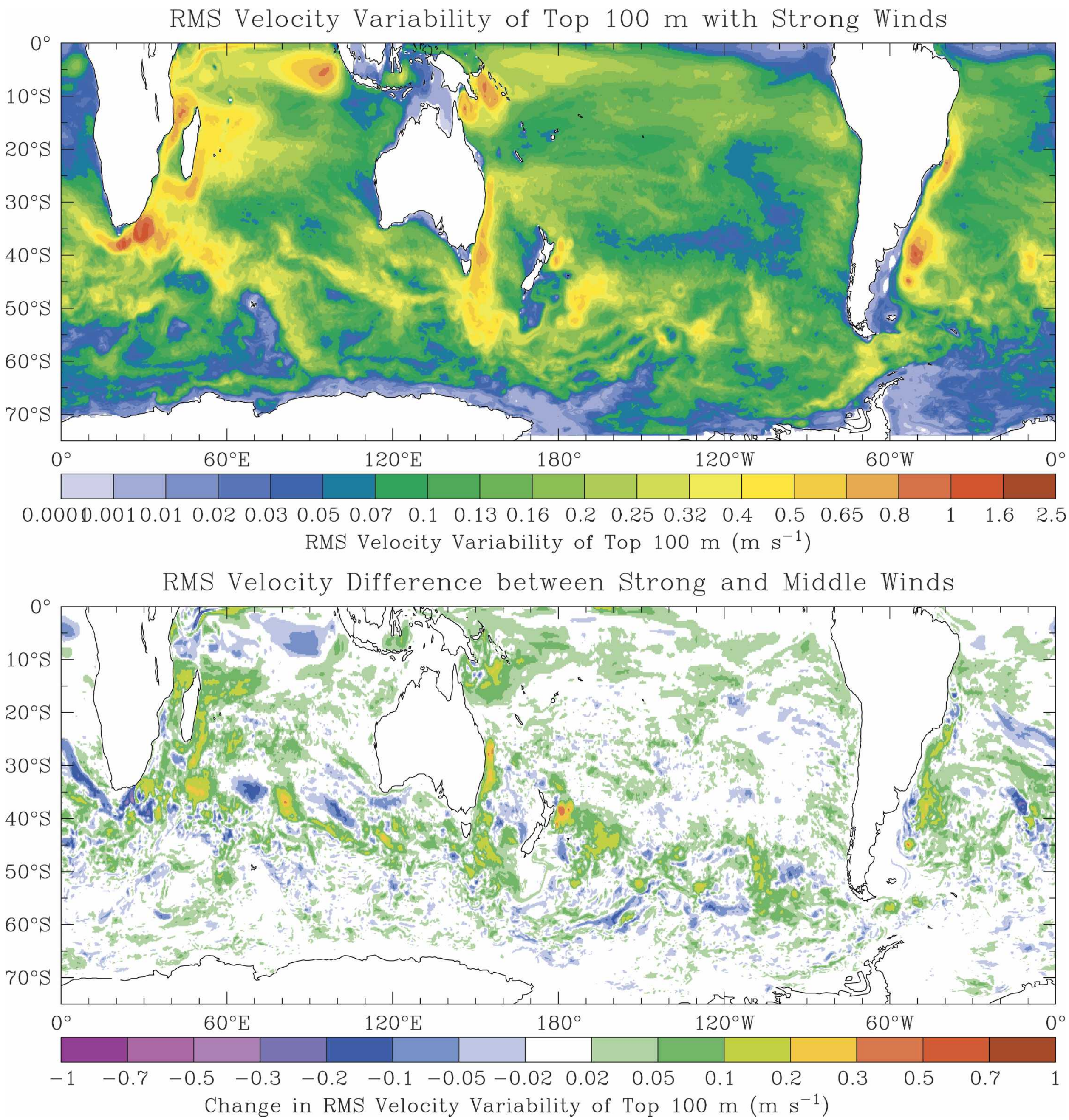

FIG. 12. (top) Surface velocity variance with strong winds and (bottom) the change in variance from changing from the middle to the strong winds for years 35–40 of the ⅙° simulations.

2003), and topography (Toggweiler and Samuels 1995; Vallis 2000) can play an important role in controlling the global stratification. This alternate view relies on the interior diffusion playing a relatively minor role. As pointed out by Huang (1999) the difference has important implications for modeling climate, since diffusion is driven by breaking internal waves, which are not themselves modeled in GCMs.

MESO does not provide a clean test of the two views of the steady-state circulation—since the strong sponges at the equator can either be interpreted as standing in for tropical diffusion within the pycnocline *or* surface transformation in the Northern Hemisphere. However, MESO does have implications for the question of the role of surface wind stress in driving the global overturning circulation. Certain papers (Mar-

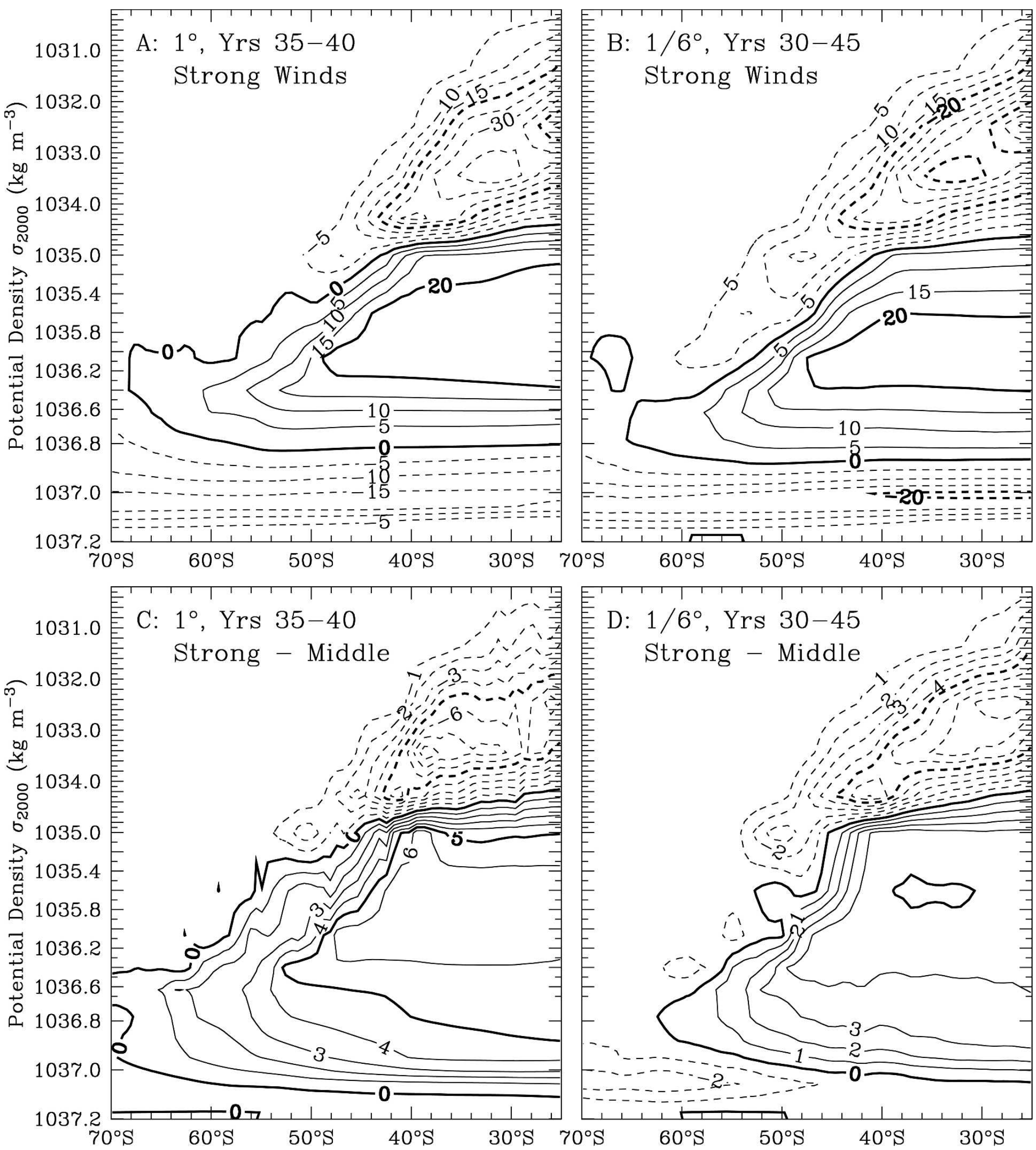

FIG. 13. The meridional overturning streamfunction in density space for the (a) 1° and (b) ⅙° resolution models with strong winds with a 5-Sv contour interval, and the changes in the overturning streamfunction between strong and middle winds with the (c) 1° and (d) ⅙° resolution models with a 1-Sv contour interval. The overturning in the 1° model includes the contribution from interface height diffusion with a coefficient of 1000 m^2 s^{-1}. The ⅙° model is averaged over 15 yr instead of 5 to reduce the influence of its much greater low-frequency variability.

shall et al. 1993; Tansley and Marshall 2001) suggest a limiting case in which changes in winds are locally compensated by changes in eddy fluxes without changing water mass transformation rates or large-scale circulation. Hallberg and Gnanadesikan (2001) found a similar limiting case when the eddy flux was much larger than the buoyancy-driven overturning. They argued, however, that in the real ocean the two fluxes were likely of comparable size, so an increase in the Ekman flux would be compensated by both an increase in water mass transformation and an increase in eddy flux. The present work supports the picture that both eddies and overturning transport changes balance changes in the winds.

It should be noted that several recent observational analyses differ substantially from the picture in which there are large fluxes of AAIW and SAMW out of the Southern Ocean. While the simulations here exhibit

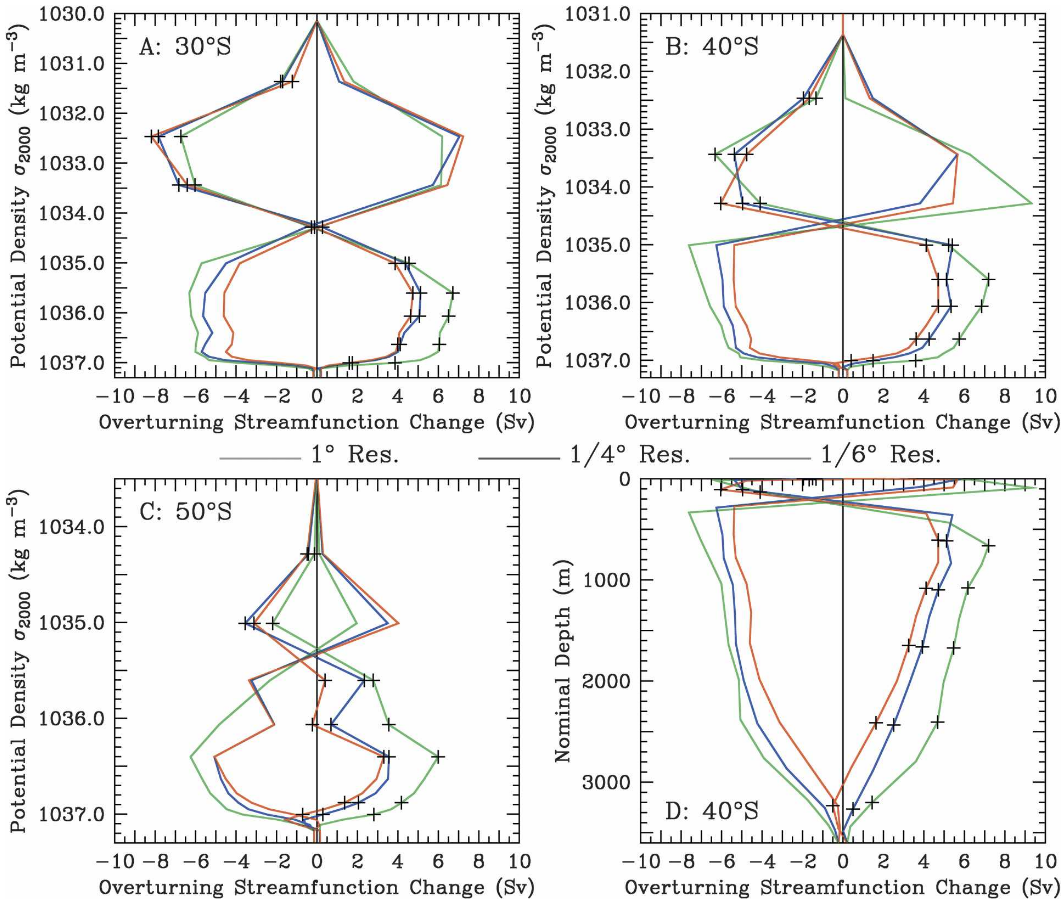

FIG. 14. Changes in zonally integrated overturning streamfunction in density space due to wind stress changes at latitudes of (a) 30°, (b) 40°, and (c) 50°S and resolutions of 1° (green), ¼° (blue), and ⅙° (red). The changes for both increasing and decreasing winds are shown in this figure; the curves from increasing winds are marked with "+" symbols. (d) Same as in (b), but with the overturning remapped to the zonal average depth of the density surfaces.

roughly 20 Sv of AAIW formation from denser waters, as compared with the 14 Sv proposed by Schmitz (1996), an inverse model by Ganachaud and Wunsch (2000) finds only 8–9 Sv of net conversion. Sloyan and Rintoul (2001), also using an inverse model, find only 3 Sv. Interestingly, they also find very little net production of waters in AAIW classes within the Southern Ocean. Talley (2003) finds essentially *no* conversion of dense waters to light waters within the Southern Ocean. In her circulation schematic, the 8 Sv of SAMW flowing northward across 30°S is basically completely fed by southward-flowing surface waters. Talley's synthesis also shows essentially no net northward flow of AAIW-class waters—the roughly 10 Sv being produced in the Atlantic and Pacific being largely balanced by southward flows in the Indian Ocean. It is worth asking whether the neglect of the eddy processes responsible for the extension of the surface cell can account for this apparent discrepancy between models and integrated analyses of data.

b. *On the parameterizability of Southern Ocean eddies*

Southern Ocean eddies clearly have a significant role in governing the overturning circulation. It is well worth inquiring whether this role can be adequately parameterized, or whether the eddies must be resolved. A common closure (equivalent to GM) is to make the eddy fluxes proportional to the thickness gradient times some thickness diffusivity, κ (i.e., $\overline{v'h'} = -\kappa\partial\bar{h}/\partial y$). The zonally integrated light transient eddy transports shown in Fig. 8 can be divided by the zonal mean meridional gradient of the thickness of the light layers to give effective diffusivities of roughly 700 m^2 s^{-1} at 55°S and 570 m^2 s^{-1} at 60°S in the ⅙° run with middle winds. With the strong winds, these values increase to roughly

850 $m^2\ s^{-1}$ at 55°S and 670 $m^2\ s^{-1}$ at 60°S, roughly proportional to the 20% increase in the squared SSH variance between the runs (Fig. 11). These diffusivities are within the range of values that can be inferred from satellite observations of the sea surface height variability (Marshall et al. 2006), and the meridional changes in the coefficient are at least in the sense suggested by the Visbeck et al. (1997) closure or the estimate of the near-surface Southern Ocean diffusivity by Karsten and Marshall (2002).

There are, however, two aspects of the calculations here that indicate that these eddy effects may be difficult to parameterize. The first is that when the winds are increased, the transient eddy fluxes increase but the zonal mean meridional thickness gradient increases only slightly at 55°S and actually decreases slightly at 60°S. The marginal eddy diffusivity that would be required to capture this response would be negative! This is contrary to the expectations from any reasonable zonal-mean parameterization of the eddy fluxes. Instead, it probably reflects the prominence of boundary current eddies in the transient eddy fluxes (see Figs. 8 and 12). These boundary eddies are driven in part by barotropic shear instability and partly by baroclinic instability that is expressed downstream of the regions of the greatest baroclinic growth rates (Hallberg and Gnanadesikan 2001). The near-surface isopycnal slopes may be mixed more passively than they would if a local baroclinic instability parameterization were apt.

A related implication of these results is that they reveal some of the weaknesses of the zonally averaged theoretical frameworks, such as Gnanadesikan (1999) or Karsten et al. (2002). Such approaches assume that the overturning circulation is dominated by transient eddies that depend on the zonally averaged state. The simulations here show (Figs. 8, 9, and 10) that there are significant eddy flow features that depend on localized processes such as eddy shedding. In this, these simulations agree with altimetric observations (Gille 1997). These processes, however, may respond differently to winds than the broadly distributed baroclinic instability in a more homogeneous region like the southeast Pacific, which appears to be much better described by a diffusive parameterization.

The other difficulty with a diffusive parameterization of the eddies is that the lower-resolution models presented here actually do include a GM-like interface height diffusivity of 1000 $m^2\ s^{-1}$—the same magnitude as the diagnosed value. The fact that the lower-resolution models with GM fail to replicate the southward extension of the subtropical cell or the sensitivity to wind stress changes of the higher model is a clear indication of the limitations of a simple interface–height diffusion parameterization. This is perhaps because the parameterization inhibits the formation of the small-scale fronts (see Figs. 6 and 9) upon which the eddy fluxes act. It is possible that a diffusive parameterization with a more sophisticated horizontal and vertical structure could lead to a coarse-resolution model that can reproduce the overturning structure and response of the eddy-permitting model. But it seems likely that there are some aspects of the overturning that will be misrepresented by any local parameterization based on baroclinic instability theory. The difference in response to changes in wind stress between the 1° run with parameterized eddies and the ⅙° run with explicit eddies suggests that the details of eddy dynamics can play an important role in the magnitude of the response of the climate system to *changes* in forcing. In other words, while it may be possible to tune models to make certain aspects of the current state of the ocean correct, it will be much more difficult to reproduce changes due to eddy activity.

5. Conclusions

It has long been known that eddies must be of leading-order importance in the Southern Ocean momentum balance, and that the World Ocean is largely filled by water masses that originate or are eroded in the Southern Ocean (Sverdrup et al. 1942). These two insights have led to two apparently contradictory views of how the circulation in the Southern Ocean is closed. As described in the introduction, the diabatic view highlights the role of water mass transformations in linking dense southward subsurface flows to the northward Ekman transport, while the adiabatic view emphasizes the role of eddies in moving momentum downward in the water column. The results here indicate that both pictures correctly describe key aspects of the circulation. There is a substantial Southern Ocean overturning circulation in the sense indicated by the diabatic view even in the presence of eddies. However, the diabatic response to changes in wind forcing is substantially attenuated by the action of a vigorous eddy field, as suggested by the adiabatic view.

The diapycnal fluxes of water in these simulations are large—more than 20 Sv of NADW is converted to AAIW and more than 30 Sv of thermocline water to SAMW or surface waters of comparable density. (The model's resolution in density is probably too coarse to clearly discriminate among the lighter water masses, and the density-space overturning does not differentiate between surface and subsurface flow.) While the lack of a seasonal cycle may be important in determining the realism of these transformations, it should be clear that the Southern Ocean mixed layer has the potential to be a major region of water mass transformation. Transient eddies play an important role in this transformation—a role that is not well described by at least one common diffusive eddy parameterization (Gent and McWilliams 1990). In the simulations shown here, they extend the cell that transforms light surface water into intermediate water far to the south (essentially to the polar front). This implies that the ocean could give up heat to the atmosphere even in latitudes where deep waters are being transformed into warmer AAIW and SAMW, and where the surface Ekman transport is northward.

Although many aspects of the mean circulation are qualitatively similar in the low-resolution (parameterized eddy) simulations and the high-resolution (eddy rich) simulations, the response of these two models to wind stress changes are markedly different. The explicit eddies lead to a substantially lighter, shallower, and weaker change in the density-space overturning than in the coarse-resolution model. Other measures of the circulation change, such as the Drake Passage transport, show a consistently smaller response with explicit eddies.

The thickness diffusivities used in the coarse-resolution simulations shown here are of approximately the right magnitude to given the correct eddy impact on the mean state. However, with this effective tuning, they appear to dramatically underpredict the eddy response to changed forcing. It is not clear that these eddy effects can be effectively parameterized—they are nonlocal in both cause and effect, and strongly dependent on details of the flow structure.

None of the simulations presented here are numerically converged with respect to the eddies. However, the changes with increasing resolutions are consistent, and it is reasonable to expect that the numerically converged (infinite resolution) solutions would exhibit even stronger differences from the coarse-resolution simulations than those shown here.

This study has examined a climatically interesting response to wind forcing only. It is not clear whether the eddy impact on the response to buoyancy forcing changes will be similar, but this is a question that should be examined.

Most important, this study emphasizes that it is imperative the oceanographic community develop and use accurate high-resolution models to examine the response of the climate system. The changes shown here would be of import for a number of climatically relevant processes, including heat transport and storage, and carbon storage in the interior. Given that the Southern Ocean has been relatively underobserved and has seen dramatic changes in its forcing in recent years, understanding the Southern Ocean response to the changing forcing is critical for correctly interpreting the observations currently being made, even to diagnose the Southern Ocean's mean circulation. Last, it is critical that climate predictions be assessed with the assistance of high-resolution ocean models to ensure the validity of their predictions.

Acknowledgments. We thank the Geophysical Fluid Dynamics Laboratory, in particular our director Ants Leetmaa, for supporting the MESO project. Isaac Held, Robbie Toggweiler, Steve Griffies, and Geoff Vallis made important contributions to the design of MESO. We are grateful to John Marshall and Kevin Speer for valuable comments on this manuscript.

APPENDIX A

Forcing the Model

Suppose that the surface temperature tendency equation is written schematically as

$$Hc_p \frac{\partial \theta}{\partial t} = M + \lambda(\theta_{\mathrm{Obs}} - \theta) + F, \tag{A1}$$

where M is the model tendency without forcing, λ is an effective damping rate (perhaps chosen to keep the model near data or perhaps from the bulk formulas), Hc_p is an effective (and as the mixed layer thickness H is not uniform, unknown) heat capacity, and F is an as yet unknown forcing rate. The long-term mean balance for a perfect model with perfect observations in a steady state would be simply $M + F = 0$. Here F is unknown, and might be diagnosed by slowly adjusting the mean flux to make it compensate for the damping term:

$$\frac{\partial F}{\partial t} = \gamma\lambda(\theta_{\mathrm{Obs}} - \theta), \tag{A2}$$

where γ is a positive definite inverse damping time scale. Here F is now a prognostic variable of the model. The steady state of Eqs. (A1) and (A2) occurs when $\theta = \theta_{\mathrm{Obs}}$ and $M + F = 0$. The unsteady behavior of these equations gives a damped oscillator with the desired final state.

Unfortunately, the results from using these equations in the model are absurd. The model admits spatial structures with much finer scales than are present in the mean state inferred from the observational datasets, and there are modest differences in the model's preferred location of a current when compared with the observations. The result is enormous diagnosed fluxes with very small spatial scales.

Instead, a much more plausible diagnosed forcing can be obtained by using

$$\frac{\partial F}{\partial t} = \gamma\lambda(\theta_{\text{Obs}} - \theta) + \gamma L^2\nabla^2 F, \tag{A3}$$

where L is a length scale below which model–observation differences are not significant. The equations are still a damped oscillator, but now the steady state is given by

$$M + F - L^2\nabla^2 F = 0 \quad \text{and} \tag{A4a}$$

$$\theta = \theta_{\text{Obs}} + (L^2/\lambda)\nabla^2 F. \tag{A4b}$$

At large scales in comparison with L, the Laplacian of the forcing is small, and the model is forced to agree with the observations. At small scales, the diagnosed forcing does not respond to model–observation discrepancies. At these smaller scales, anything but a full coupled model is likely to be wildly inaccurate because of the strong interactions between the two boundary layers. Thus, placing a lower cutoff on the scales where the restoring operates would seem to reduce the spurious impact on the dynamics. For the simulations described in this manuscript, L is set to 200 km—about the scale of Southern Ocean jet separation. Here γ is set to $1/120$ days—long when compared with the typical eddy time scale but short enough for the fluxes to be fully diagnosed within the spinup period of these runs.

The traditional approach of simple damping (setting F to 0) leads to a steady state with a substantial persistent error. Instead, a mean flux is sometimes diagnosed by repeatedly averaging the damping flux of a run and then using it to adjust the mean flux for the next run. The method described here is qualitatively similar to a large number of such iterations.

REFERENCES

Andrews, D. G., and M. E. McIntyre, 1976: Planetary waves in horizontal and vertical shear: The generalized Eliassen-Palm relation and the mean zonal acceleration. *J. Atmos. Sci.,* **33,** 2031–2048.

Arakawa, A., and Y.-J. G. Hsu, 1990: Energy conserving and potential-enstrophy dissipating schemes for the shallow water equations. *Mon. Wea. Rev.,* **118,** 1960–1969.

Best, S. E., V. O. Ivchenko, K. J. Richards, R. D. Smith, and R. C. Malone, 1999: Eddies in numerical models of the Antarctic Circumpolar Current and their influence on the mean flow. *J. Phys. Oceanogr.,* **29,** 328–350.

Bryan, F., 1987: Parameter sensitivity of primitive equation ocean general circulation models. *J. Phys. Oceanogr.,* **17,** 970–985.

Cunningham, S. A., S. G. Alderson, B. A. King, and M. A. Brandon, 2003: Transport and variability of the Antarctic Circumpolar Current in Drake Passage. *J. Geophys. Res.,* **108,** 8084, doi:10.1029/2001JC001147.

Doney, S. C., W. G. Large, and F. O. Bryan, 1998: Surface ocean fluxes and water mass transformations in the coupled NCAR Climate System Model. *J. Climate,* **11,** 1420–1441.

Döös, K., and D. J. Webb, 1994: The Deacon cell and the other meridional cells of the Southern Ocean. *J. Phys. Oceanogr.,* **24,** 429–442.

Easter, R. C., 1993: Two modified versions of Bott's positive-definite numerical advection scheme. *Mon. Wea. Rev.,* **121,** 297–304.

Ferrari, R., and A. Plumb, 2003: Residual circulation in the ocean. *Near Boundary Processes and Their Parameterization: Proc. 2003 'Aha Huliko'a Hawaiian Winter Workshop,* Honolulu, HI, University of Hawaii at Manoa, 219–228.

Ganachaud, A., and C. Wunsch, 2000: The oceanic meridional overturning circulation, mixing, bottom water formation, and heat transport. *Nature,* **408,** 453–457.

Gent, P., and J. C. McWilliams, 1990: Isopycnal mixing in ocean models. *J. Phys. Oceanogr.,* **20,** 150–155.

——, J. Willebrand, T. J. McDougall, and J. C. McWilliams, 1995: Parameterizing eddy-induced tracer transports in ocean circulation models. *J. Phys. Oceanogr.,* **25,** 463–474.

——, W. G. Large, and F. O. Bryan, 2001: What sets the mean transport through Drake Passage? *J. Geophys. Res.,* **106,** 2693–2712.

Gille, S. T., 1997: The Southern Ocean momentum balance: Evidence for topographic effects from numerical model output and altimeter data. *J. Phys. Oceanogr.,* **27,** 2219–2232.

Gnanadesikan, A., 1999: A simple theory for the structure of the oceanic pycnocline. *Science,* **283,** 2077–2079.

——, and R. W. Hallberg, 2000: The relationship of the Circumpolar Current to Southern Hemisphere winds in coarse-resolution ocean models. *J. Phys. Oceanogr.,* **30,** 2013–2034.

——, R. D. Slater, and B. L. Samuels, 2003: Dependence of oceanic heat transport and watermass transformation on subgridscale parameterization in coarse-resolution ocean models. *Geophys. Res. Lett.,* **30,** 1967, doi:10.1029/2003GL018036.

Griffies, S. M., 1998: The Gent–McWilliams skew flux. *J. Phys. Oceanogr.,* **28,** 832–842.

——, and R. W. Hallberg, 2000: Biharmonic friction with a Smagorinsky-like viscosity for use in large-scale eddy-permitting ocean models. *Mon. Wea. Rev.,* **128,** 2935–2946.

——, A. Gnanadesikan, R. C. Pacanowski, V. D. Larichev, R. D. Smith, and J. K. Dukowicz, 1998: Isoneutral mixing in level-coordinate ocean models. *J. Phys. Oceanogr.,* **28,** 805–830.

——, R. C. Pacanowski, and R. W. Hallberg, 2000: Spurious diapycnal mixing associated with advection in a *Z*-coordinate ocean model. *Mon. Wea. Rev.,* **128,** 538–564.

Hallberg, R., 1995: Some aspects of the circulation in ocean basins with isopycnals intersecting the sloping boundaries. Ph.D. thesis, University of Washington, 244 pp.

——, 1997: Stable split time-stepping schemes for large-scale ocean modeling. *J. Comput. Phys.,* **135,** 946–952.

——, 2000: Time integration of diapycnal diffusion and Richardson number–dependent mixing in isopycnal coordinate ocean models. *Mon. Wea. Rev.,* **128,** 1402–1419.

——, 2003: The suitability of large-scale ocean models for adapting parameterizations of boundary mixing and a description of a refined bulk mixed layer model. *Near Boundary Processes and Their Parameterization: Proc. 2003 'Aha Huliko'a Hawaiian Winter Workshop,* Honolulu, HI, University of Hawaii at Manoa, 187–203.

——, 2005: A thermobaric instability of Lagrangian vertical coordinate ocean models. *Ocean Modell.,* **8,** 279–300.

——, and A. Gnanadesikan, 2001: An exploration of the role of transient eddies in determining the transport of a zonally reentrant current. *J. Phys. Oceanogr.,* **31,** 3312–3330.

Held, I. M., and T. Schneider, 1999: The surface branch of the zonally averaged mass transport circulation in the troposphere. *J. Atmos. Sci.,* **56,** 1688–1697.

Hirst, A. C., and T. J. McDougall, 1998: Meridional overturning and dianeutral motion in a *z*-coordinate ocean model including eddy-induced advection. *J. Phys. Oceanogr.,* **28,** 1205–1223.

Huang, R. X., 1999: Mixing and energetics of the oceanic thermohaline circulation. *J. Phys. Oceanogr.,* **29,** 727–746.

Johnson, G. C., and H. Bryden, 1989: On the strength of the Circumpolar Current. *Deep-Sea Res.,* **36,** 39–53.

Karsten, R., and J. Marshall, 2002: Constructing the residual circulation of the Antarctic Circumpolar Current from observations. *J. Phys. Oceanogr.,* **32,** 3315–3327.

——, H. Jones, and J. Marshall, 2002: The role of eddy transfer in setting the stratification and transport of a Circumpolar Current. *J. Phys. Oceanogr.,* **32,** 39–54.

Killworth, P. D., and M. M. Nanneh, 1994: Isopycnal momentum budget of the Antarctic Circumpolar Current in the Fine Resolution Antarctic Model. *J. Phys. Oceanogr.,* **24,** 1201–1223.

Klinger, B. A., and J. Marotzke, 1999: Behavior of double-hemisphere thermohaline flows in a single basin. *J. Phys. Oceanogr.,* **29,** 382–399.

——, S. Drijfhout, J. Marotzke, and J. R. Scott, 2003: Sensitivity of basinwide meridional overturning to diapycnal diffusion and remote wind forcing in an idealized Atlantic–Southern Ocean geometry. *J. Phys. Oceanogr.,* **33,** 249–266.

Kraus, E. B., and J. S. Turner, 1967: A one-dimensional model of the seasonal thermocline. II: The general theory and its consequences. *Tellus,* **19,** 98–106.

MacCready, P., and P. Rhines, 2001: Meridional transport across a zonal channel: Topographic localization. *J. Phys. Oceanogr.,* **31,** 1427–1439.

Marshall, D., 1997: Subduction of water masses in an eddying ocean. *J. Mar. Res.,* **55,** 201–222.

Marshall, J., and T. Radko, 2003: Residual-mean solutions for the Antarctic Circumpolar Current and its associated overturning circulation. *J. Phys. Oceanogr.,* **33,** 2341–2354.

——, D. Olbers, H. Ross, and D. Wolf-Gladrow, 1993: Potential vorticity constraints on the dynamics and hydrography of the Southern Ocean. *J. Phys. Oceanogr.,* **23,** 465–487.

——, E. Shuckburgh, H. Jones, and C. Hill, 2006: Estimates and implications of surface eddy diffusivity in the Southern Ocean derived from tracer transport. *J. Phys. Oceanogr.,* **36,** 1806–1821.

McDermott, D. A., 1996: The regulation of northern overturning by Southern Hemisphere winds. *J. Phys. Oceanogr.,* **26,** 1234–1255.

McDougall, T. J., and P. C. McIntosh, 2001: The temporal-residual-mean velocity. Part II: Isopycnal interpretation and the tracer and momentum equations. *J. Phys. Oceanogr.,* **31,** 1222–1246.

Nof, D., 2000: Does wind control the import and export of the South Atlantic? *J. Phys. Oceanogr.,* **30,** 2650–2667.

Redi, M., 1982: Oceanic isopycnal mixing by coordinate rotation. *J. Phys. Oceanogr.,* **12,** 1154–1158.

Renwick, J. A., 2004: Trends in the Southern Hemisphere polar vortex in NCEP and ECMWF reanalyses. *Geophys. Res. Lett.,* **31,** L07209, doi:10.1029/2003GL19302.

Rhines, P. B., 1977: The dynamics of unsteady currents. *The Sea,* E. Goldberg, Ed., Marine Modeling, Vol. 6, Wiley, 189–318.

Schmitz, W. J., 1996: On the World Ocean Circulation. Vol. 1: Some Global Features/North Atlantic Circulation. Woods Hole Oceanographic Institute Tech. Rep. WHOI-96-03. 141 pp.

Semtner, A. J., and R. M. Chervin, 1992: Ocean general-circulation from a global eddy-resolving model. *J. Geophys. Res.,* **97,** 5493–5550.

Sloyan, B., and S. R. Rintoul, 2001: Circulation, renewal, and modification of Antarctic Mode and Intermediate Water. *J. Phys. Oceanogr.,* **31,** 1005–1030.

Smith, W. H. F., and D. T. Sandwell, 1997: Global sea floor topography from satellite altimetry and ship depth soundings. *Science,* **277,** 1956–1962.

Speer, K. G., B. Sloyan, and S. R. Rintoul, 2000: The diabatic Deacon Cell. *J. Phys. Oceanogr.,* **30,** 3212–3222.

Stevens, D. P., and V. O. Ivchenko, 1997: The zonal momentum balance in a realistic, eddy resolving general circulation model of the Southern Ocean. *Quart. J. Roy. Meteor. Soc.,* **123,** 929–951.

Sun, S., R. Bleck, C. Rooth, J. Dukowicz, E. Chassignet, and P. Killworth, 1999: Inclusion of thermobaricity in isopycnic-coordinate ocean models. *J. Phys. Oceanogr.,* **29,** 2719–2729.

Sverdrup, H. U., M. W. Johnson, and R. H. Flemming, 1942: *The Oceans: Their Physics, Chemistry and General Biology*. Prentice Hall, 1087 pp.

Talley, L. D., 2003: Shallow, intermediate, and deep overturning components of the global heat budget. *J. Phys. Oceanogr.,* **33,** 530–560.

Tansley, C., and D. Marshall, 2001: On the dynamics of wind-driven circumpolar currents. *J. Phys. Oceanogr.,* **31,** 3258–3271.

Thompson, L., K. Kelly, D. Darr, and R. Hallberg, 2002: Buoyancy and mixed layer effects on the sea surface height response in an isopycnal model of the North Pacific. *J. Phys. Oceanogr.,* **32,** 3657–3670.

Toggweiler, J. R., and B. L. Samuels, 1993: New radiocarbon constraints on the upwelling of abyssal water to the ocean's surface. *The Global Carbon Cycle,* M. Heimann, Ed., Springer-Verlag, 333–365.

——, and ——, 1995: Effect of Drake Passage on the global thermohaline circulation. *Deep-Sea Res. I,* **42,** 477–500.

——, and ——, 1998: On the ocean's large-scale circulation near the limit of no vertical mixing. *J. Phys. Oceanogr.,* **28,** 1832–1852.

——, and H. Bjornsson, 2000: Drake Passage and paleoclimate. *J. Quart. Sci.,* **15,** 319–328.

Trenberth, K. E., and J. M. Caron, 2001: Estimates of meridional atmosphere and ocean heat transports. *J. Climate,* **14,** 3433–3443.

Vallis, G. K., 2000: Large-scale circulation and production of stratification: Effects of wind, geometry, and diffusion. *J. Phys. Oceanogr.,* **30,** 933–954.

Veronis, G., 1996: Effect of a constant, zonal wind on wind-driven ocean circulation. *J. Phys. Oceanogr.,* **26,** 2525–2528.

Visbeck, M., J. Marshall, T. Haine, and M. Spall, 1997: Specification of eddy transfer coefficients in coarse-resolution ocean circulation models. *J. Phys. Oceanogr.,* **27,** 381–402.

Warren, B., J. LaCasce, and P. A. Robbins, 1996: On the obscurantist physics of "form drag" in theorizing about the Circumpolar Current. *J. Phys. Oceanogr.,* **26,** 2297–2301.

Whitworth, T., III, W. D. Nowlin, and S. J. Worley, 1982: The net transport of the Antarctic Circumpolar Current through Drake Passage. *J. Phys. Oceanogr.,* **12,** 960–971.

Young, W. R., 1994: The subinertial mixed layer approximation. *J. Phys. Oceanogr.,* **24,** 1812–1826.